Stem Cell Research 17 (2016) 296–305

Contents lists available at ScienceDirect

Stem Cell Research

journal homepage: www.elsevier.com/locate/scr

Robust reprogramming of Ataxia-Telangiectasia patient and carrier erythroid cells to induced pluripotent stem cells

Niraj Bhatt [a,1], Rajib Ghosh [a,1], Sanchita Roy [a,1], Yongxing Gao [b], Mary Armanios [c], Linzhao Cheng [b], Sonia Franco [a,*]

[a] Department of Radiation Oncology and Molecular Radiation Sciences, and the Sidney Kimmel Comprehensive Cancer Center, Johns Hopkins University School of Medicine, Baltimore, MD 21287, USA

[b] Division of Hematology, Department of Medicine, and the Institute for Cell Engineering, Johns Hopkins University School of Medicine, Baltimore, MD 21287, USA

[c] Department of Oncology, the Sidney Kimmel Comprehensive Cancer Center and the McKusick Nathans Institute of Genetic Medicine, Johns Hopkins University School of Medicine, Baltimore, MD 21287, USA

ARTICLE INFO

Article history:
Received 29 February 2016
Received in revised form 29 July 2016
Accepted 6 August 2016
Available online 12 August 2016

Keywords:
induced pluripotent stem cells
Ataxia-Telangiectasia
ATM
radiation
telomere
teratoma

ABSTRACT

Biallelic mutations in ATM result in the neurodegenerative syndrome Ataxia-Telangiectasia, while ATM haploinsufficiency increases the risk of cancer and other diseases. Previous studies revealed low reprogramming efficiency from A-T and carrier fibroblasts, a barrier to iPS cell-based modeling and regeneration. Here, we tested the feasibility of employing circulating erythroid cells, a compartment no or minimally affected in A-T, for the generation of A-T and carrier iPS cells. Our results indicate that episomal expression of Yamanaka factors plus BCL-xL in erythroid cells results in highly efficient iPS cell production in feeder-free, xeno-free conditions. Moreover, A-T iPS cells generated with this protocol maintain long-term replicative potential, stable karyotypes, re-elongated telomeres and capability to differentiate along the neural lineage *in vitro* and to form teratomas *in vivo*. Finally, we find that haploinsufficiency for ATM does not limit reprogramming from human erythroid cells or *in vivo* teratoma formation in the mouse.

1. Introduction

Ataxia-Telangiectasia (A-T; OMIM208900) is an autosomal recessive syndrome caused by compound heterozygous null mutations in the locus encoding the ATM kinase at chromosome 11q22 (Savitsky et al., 1995) ("classical" A-T). Most A-T patients suffer from severe cerebellar degeneration due to Purkinje cell death, B and T cell immunodeficiency and increased cancer predisposition (Boder and Sedgwick, 1958; Lavin, 2008; McKinnon, 2012; Shiloh, 2003). Moreover, haploinsufficiency for ATM, estimated to occur in 1.5-2% of the population worldwide (Swift et al., 1986), increases the risk of cancer and heart disease and decreases lifespan (Su and Swift, 2000; Swift and Chase, 1983). However, how alterations in ATM copy number result in such pleiotropic phenotypes remains incompletely understood.

Nucleoplasmic ATM is activated in response to DNA double-strand breaks (DSB) to orchestrate the cellular DNA Damage Response (DDR) and promote cell cycle checkpoint activation and DSB repair (Paull, 2015; Shiloh and Ziv, 2013). In ATM-deficient developing lymphocytes, broken DNA ends at "programmed" DSBs remain unrepaired or are repaired aberrantly, leading to T and B cell immunodeficiency and oncogenic translocations, respectively (Callen et al., 2007; Franco et al., 2006). In contrast, the contribution of defective DSB repair to the neurodegenerative phenotypes observed in A-T is less well understood. In this context, the finding that ATM may localize primarily to the cytoplasm in post-mitotic neurons (Barlow et al., 2000; Oka and Takashima, 1998), together with its emerging cytoplasmic functions in the regulation of oxidative stress and metabolism (Ambrose and Gatti, 2013; Paull, 2015; Valentin-Vega et al., 2012; Zhang et al., 2015), may suggest a mechanism independent of DSB repair (Carlessi et al., 2013). However, $Atm^{-/-}$ mice (Lavin, 2013) and $ATM^{-/-}$ pigs (Beraldi et al., 2015) do not manifest ataxia or significant cerebellar pathology, underscoring the need for novel human cell-based approaches to model neurodegeneration.

Induced pluripotent stem (iPS) cells derived from human somatic cells by expression of defined transcription factors represent a powerful novel system for disease modeling (Park et al., 2008; Takahashi et al., 2007). Moreover, the recent development of highly efficient genome editing tools has greatly facilitated the use of corrected iPS cell-derived products for autologous tissue replacement (Mali and Cheng, 2012). Most relevant to A-T, preclinical studies have started to define sets of transcription factors that promote differentiation of mouse ES cells (Muguruma et al., 2010; Tao et al., 2010) and human ES and iPS cells (Muguruma et al., 2015; Wang et al., 2015) to Purkinje neurons.

DOI of original article: http://dx.doi.org/10.1016/j.scr.2016.08.003.
* Corresponding author at: 1550 Orleans St, CRBII room 405, Baltimore, MD 21287, USA.
E-mail address: sfranco2@jhmi.edu (S. Franco).
[1] These authors contributed equally to this work.

http://dx.doi.org/10.1016/j.scr.2016.08.006

Furthermore, these cells have some engraftment capability (Muguruma et al., 2010; Wang et al., 2015), suggesting that A-T iPS cells could similarly represent a source of neuronal cells for disease modeling and ultimately for regenerative therapy.

Previous work has shown that A-T iPS cells generated by expression of Yamanaka factors in A-T fibroblasts (Fukawatase et al., 2014; Lee et al., 2013; Nayler et al., 2012) or T cells (Lin et al., 2015) are viable. However, all fibroblast-based protocols employed integrating viral vectors and feeder layers (Fukawatase et al., 2014; Lee et al., 2013; Nayler et al., 2012). Moreover, consistent with impaired reprogramming in fibroblasts deficient for other DSB repair factors (Gonzalez et al., 2013; Tilgner et al., 2013), the efficiency of reprogramming from A-T fibroblasts was decreased about 100-fold relative to control fibroblasts from healthy individuals (Fukawatase et al., 2014; Lee et al., 2013; Nayler et al., 2012). Furthermore, the efficiency of reprogramming from A-T carrier fibroblasts was also markedly decreased in one study (Nayler et al., 2012), suggesting a gene dose effect. Patient-derived circulating T lymphocytes were recently shown to represent an alternative to fibroblasts (Lin et al., 2015). However, the fact that they often harbor clonal pre-leukemic rearrangements involving antigen receptor loci (Taylor et al., 1996) complicates their use for disease modeling and therapy. In this context, reprogramming of nonlymphoid mononuclear cells (Chou et al., 2015; Dowey et al., 2012; Hu et al., 2011) could provide a robust yet safe approach for A-T patients and carriers. More specifically, the erythroid compartment is no or minimally affected in A-T (Boder and Sedgwick, 1958).

Here, we show that A-T and carrier circulating erythroid cells can be reprogrammed to iPS cells in xeno-free, feeder-free conditions with high efficiency. Moreover, this protocol results in A-T iPS cells with intact replicative potential, stable karyotypes, re-elongated telomeres and capability to differentiate along the neural lineage.

2. Materials and Methods

2.1. Patients

A 12 year-old male diagnosed with A-T and followed at the A-T Clinic at Johns Hopkins Hospital and his parents were consented and enrolled in this study, following protocols approved by the Johns Hopkins Institutional Review Board (IRB#CR00007000). The proband was known to be compound heterozygous for frameshift mutations in exon 23 (3369delA, codon 1123) and exon 26 (3754delTATinsCA in codon 1252) of *ATM*, both resulting in a null allele. Peripheral blood was drawn by venipuncture and subjected to reprogramming, as described below. The iPS cell lines generated from this family were designated as SF-001 (mother), SF-002 (father) and SF-003 (patient). The BC1 iPS cell line was previously generated in the laboratory of L.C. from bone marrow (BM) $CD34^+$ cells of an adult healthy donor (Chou et al., 2011).

2.2. Generation of iPS cells from peripheral blood erythroid cells

Reprogramming was done in the laboratory of L.C. as previously described (Chou et al., 2015; Dowey et al., 2012). In brief, mononuclear cells (MNCs) were isolated from PB (15 to 30 mL per donor) using a Ficoll gradient and cultured for one week in serum-free media containing Stem Cell Factor (SCF; 255-SC, 50 ng/mL, R&D Systems, Minneapolis MN), interleukin (IL)-3 (10 ng/mL, product number 200-03, PreproTech, Rocky Hill NJ) and erythropoietin (2 U/mL; National Drug Code (NDC) 59,676-303-01), to promote erythroblast expansion, as we have previously described (Chou et al., 2015). Cells were then transfected with three episomal plasmids encoding Yamanaka factors (OCT4, SOX2, KLF4 and c-MYC) and BCL-xL and cultured for two additional weeks in reprogramming medium. At day 14 after reprogramming, cells were stained with an antibody to TRA-1-60 and the total number of positive and negative colonies was counted. To enrich cultures for iPS cells, TRA1-60^+ cells were sorted and pooled for expansion.

2.3. Cell culture

Human iPS cells were cultured in Essential 8 Medium (Invitrogen A1517001) in 6-well plates coated with vitronectin (VTN-N; Invitrogen A14700). For passage, cells were disaggregated using StemPro Accutase Cell Dissociation Reagent (Thermo Fisher Scientific, #A11105). A ROCK inhibitor Y-27,632 dihydrochloride (Santa Cruz Biotechnology; sc-281,642 A) was added during passage at a concentration of 10 μM.

2.4. In vivo iPS cell immunostaining

iPS cells were incubated with antibodies to pluripotency markers OCT4, SOX2, SSEA4 and TRA-1-60 using the Pluripotent Stem Cells 4-marker Immunocytochemistry Kit (Life Technologies, A24881), following manufacturer's instructions. Images were taken using an EVOS FL Auto Cell Imaging System.

2.5. Teratoma assay

iPS cells (5-10 million) were mixed 1:1 with Matrigel (Cornig Matrigel hESC-qualified Matrix, #354,277) to a total volume of 200μL and injected into the flanks of NOD scid gamma (NGS) mice subcutaneously. After 2-34 weeks, teratomas were harvested, fixed in formalin and embedded in parafin at the Johns Hopkins Histopathology Core Facility. Five hematoxilyn/eosin (H/E)-stained sections were analyzed for lineage.

2.6. Analysis of mutation by sequencing

For confirmation of ATM mutations, we amplified genomic DNA from iPS cell lines using the following primers: for exon 23, ATM-23F: 5′- TTTGTTCTGGAATATGCTTTGG-3′ and ATM-23R: 5′-TGGTGAAGTAATTTATGGGATATT CA-3′; for exon 26, ATM-26F: 5′- CTT TAATGCTGATGGTATTAAAACAG-3′ and ATM-26-R: 5′-GCCATACCTGTTTTCCCAAT-3′. For mutational analysis of the p53 locus in line SF-001, we amplified genomic DNA at exons 5-8 of p53 using previously described primers (Rechsteiner et al., 2013): ex5-F: 5′-CACTTGTGCCCTGACTTTCA-3′; ex5-R: 5′-AACCAGCCCTGTCGTCTCT-3′; ex6-F: 5′-CAGGCCTCTGATTCCTCACT-3′; ex6-R: 5′-CTTAACCCCTCCTCCCAGAG-3′; ex7-F; 5′-CCACAGGTCTCCCCAAGG-3′; ex7-R: 5′-CAGCAGGCCAGTGTGCAG-3′; ex8-F: 5′-GCCTCTTGCTTCTCTTTTCC-3′; ex8-R: 5′-TAACTGCACCCTTGGTCTCC-3′. For both, PCR products were purified, cloned into TOPO-TA and sequenced.

2.7. Plasmid integration analyses

To exclude plasmid integration, genomic DNA was amplified with primers specific to the common plasmid backbone: EBNA-Fw1: 5′-ACGATGCTTTCCAAACCACC-3′ and EBNA-Rev1: 5′-CATCATCATCCGGGTCTCCA-3′. As a control, we amplified the same DNA with primers to 18S: 18S-F: 5′-GCGAGTACTCAACACCAACATCG-3′ and 18S-R: 5′-TCAAGTCTCCCCAGCCTTGC-3′.

2.8. Short Tandem Repeat (STR) Profiling

To confirm line identity, Short Tandem Repeat (STR) profiling was done for all lines at early passage at the Johns Hopkins Genetic Resources Core Facility, using GenePrint10 (Promega).

2.9. X-ray irradiation

Cells were either mock-irradiated or irradiated using a CIXD X-Ray irradiator (dual x-ray tube system), Xstrahl Ltd., UK, operating at a dose rate of 3.93 Gy/min.

2.10. Immunoblotting

iPS cells were resuspended in RIPA buffer supplemented with PMSF, protease inhibitors and the phosphatase inhibitors sodium fluoride, sodium orthovanadate and β-glycerophosphate. One hundred μg of protein were resolved via SDS-PAGE, transferred to PVDF membranes and blotted with antibodies to the following proteins: γ-H2AX (clone JBW301, Millipore); ATM (Millipore, #071,286), phospho-ATM (Ser1981) (clone 10H11.E12, Millipore), p53 (clone 1C12, Cell Signaling), phospho-p53 (Ser15) (Cell Signaling), KAP1 (Abcam, ab10484) and phospho-KAP1 (Ser284) (Bethyl Laboratories, A300-767 A). Secondary antibodies were HRP-linked anti-mouse (Cell Signaling; 7076) and HRP-linked anti-rabbit IgG (Cell Signaling; 7074). To control for loading, blots were hybridized with an HRP-conjugated antibody to GAPDH (clone 14C10; Cell Signaling, #3683S).

2.11. Indirect immunofluorescence

iPS cells were disaggregated into single-cell suspensions were spun onto slides using a Shandon cytospin. After drying, cells were fixed in 4% paraformaldehyde, permeabilized in 0.3% Triton-X, blocked in 3% BSA for 20 min and incubated with the following primary antibodies: phospho-ATM (Ser1981; clone10H11.12; Millipore), γ-H2AX (clone JBW301; Millipore) and 53BP1 (Novus Biologicals, NB100-34). Secondary antibodies were Cy3-conjugated goat anti-mouse IgG (115-166-071, Jackson ImmunoResearch), Cy3-conjugated goat anti-rabbit IgG (111-166-003; Jackson Immunoresearch), AlexaFluor 488-conjugated goat anti-mouse IgG (A-11,029; Invitrogen) and AlexaFluor 488-conjugated goat anti-rabbit IgG (A-11,034; Invitrogen). Slides were mounted in Vectashield with DAPI (Vector Laboratories). Images were acquired using a Zeiss Axioplan Imager Z.1 microscope equipped with a Zeiss AxioCam and an HXP120 mercury lamp (Jena GbH) and analyzed using dedicated software (Zeiss Axiovision Rel4.6). At least 50 cells per slide were counted.

2.12. Quantification of telomere length by flowFISH

Telomere length was measured in the lab of M.A. on peripheral blood lymphocytes using flow cytometry and fluorescence in situ hybridization (flowFISH) as previously described (Baerlocher et al., 2006). The lymphocyte and granulocyte telomere length values were then plotted on a nomogram derived from a cohort of 192 healthy controls as shown (Alder et al., 2015). Telomere length was measured on iPS cells similarly using the flowFISH method and comparisons of were made between cells 12 passages apart.

2.13. Quantification of telomere length by FISH on metaphases

iPS cells were incubated in 0.1 μg/mL colcemid (KaryoMAX, Gibco) for 4 h, swollen in 0.45% KCl for 30 min at 37 °C and fixed in methanol/acetic acid (3/1). Metaphases were hybridized with a telomere peptic nucleic acid (PNA) probe as described and analyzed as described (Orsburn et al., 2010). For quantitative analysis of telomere length on metaphases, we employed TFL-Telo software (kind gift of Dr. Peter Lansdorp). We analyzed 10 metaphases per sample.

2.14. Quantitative RT-PCR for hTERT

For gene expression analyzes of hTERT, 2 mg of total RNA from each sample was reverse transcribed using the SuperScript® VILO cDNA Synthesis Kit (Thermo Fisher Scientific Inc. Waltham, MA) and oligo(dT)20 primers. All qPCR experiments were performed using ddCt method and Power SYBR Green Master Mix (Applied Biosystems, Carlsbad, CA) on a CFX384 BioRad Real-Time PCR System (BioRad, Hercules, CA). 18S was used as the endogenous control. Primers were: hTERT-F: 5′-CGCCAGCATCATCAAACCCC-3′, hTERT-R: 5′-CTGCAGGTGAGCCACGAACT-3′, 18S-F: 5′-GATGGGCGGCGGAAAATAG-3′; 18S-R: 5′-GCGTGGATTCTGCATAATGGT-3′.

2.15. Karyotyping by G-banding

iPS cell lines SF-002 (P10) and SF-003 (P8) were sent to the WiCell Genetic Laboratory for metaphase preparation and G banding. For each line, 20 metaphases were analyzed.

2.16. Gene Expression Analysis

RT^2 Profiler™ PCR Array for Human Induced Pluripotent Stem Cells (PAHS-092Z, Qiagen) was used to analyze level of pluripotency in SF-003 and control BC1 and SF-002 iPS cell lines. Total RNA was reverse-transcribed into cDNA using SuperScript® IV Reverse Transcriptase System (Thermo Fisher Scientific Inc. Waltham, MA) and oligo(dT)20 primers. The real time RT-PCR reaction was performed on a CFX384 BioRad Real-Time PCR System (BioRad, Hercules, CA) and data was analyzed using the RT^2 Profiler PCR array data analysis platform provided by the manufacturer (Qiagen, Valencia, CA).

2.17. Differentiation of iPS cells to Neural Stem Cells (NSC)

Human iPS cell cultures at approximately 20-25% confluency were grown in Pluripotent Stem Cell (PSC) Neural Induction Medium (for 500 mL, 490 mL of Neurobasal Medium and 10 mL of Neural Induction Supplement; Gibco, A1647801). After 6 days, P0 NSCs were harvested and expanded in Neural Expansion Medium (for 100 mL, 49 mL of Neurobasal Medium, 2 mL of Neural Induction Supplement and 49 mL of Advanced DMEM/F-12 (Gibco, 12,634,010). ROCK inhibitor Y27632 at a concentration of 5 μM was added during the first night. After 4 days, P1 NSC cultures were stained with antibodies to nestin and SOX1 using the Human Neural Stem Cell Immunocytochemistry Kit (Gibco, A24354), following manufacturer's instructions. Cells were counterstained with DAPI and imaged in a Nikon Eclipse TE200 microscope.

2.18. In vivo teratoma formation assay in 4iF-A/Atm mice

The i4F-A mouse strain carrying two transgenes, one expressing "Yamanaka factors" OCT4, SOX2, KLF4 and c-MYC under a TetO promoter and one expressing the transcriptional activator rtTA (Abad et al., 2013), was obtained from Jackson Laboratories (stock# 023,749). A previously described strain of $Atm^{+/-}$ mice (Barlow et al., 1996), also in a C57BL/6 background, was obtained from Jackson Laboratories (stock 008,536). All experiments were done in 2-4 month old mice. Males and females were used at similar ratios. Teratomas were induced as previously described (Abad et al., 2013). Mouse health was monitored daily and moribund animals were euthanized and necropsied. All animal studies were conducted in accordance with NIH guidelines and Institutional Animal Care and Use Committee (IACUC)-approved protocols.

2.19. Statistical analysis

Mice survival data was presented in Kaplan Meier curves and analyzed using the log-rank test. For cellular experiments, data was presented as the mean and either the standard deviation (s.d.) or the standard error of the mean (s.e.m.) of at least 3 replicas, as indicated. Statistical significance was calculated using Student's *t*-test.

3. Results

3.1. Generation of A-T and carrier iPS cells from circulating erythroid cells is highly efficient

To test the feasibility of using patient-derived erythroblasts as a source of A-T iPS cells, we expressed Yamanaka factors plus BCL-xL in *in vitro* expanded erythroid cells of an A-T patient (see Fig. 1A for pedigree and iPS cell line nomenclature; Fig. 1B for schematic of the ATM locus and disease-causing mutations). BCL-xL was added because previous work in the laboratory of L.C. demonstrated that, in the same experimental conditions employed here, it markedly increases the efficiency of reprogramming of blood erythroid cells, relative to expression of Yamanaka factors alone (Chou et al., 2015). In parallel, we

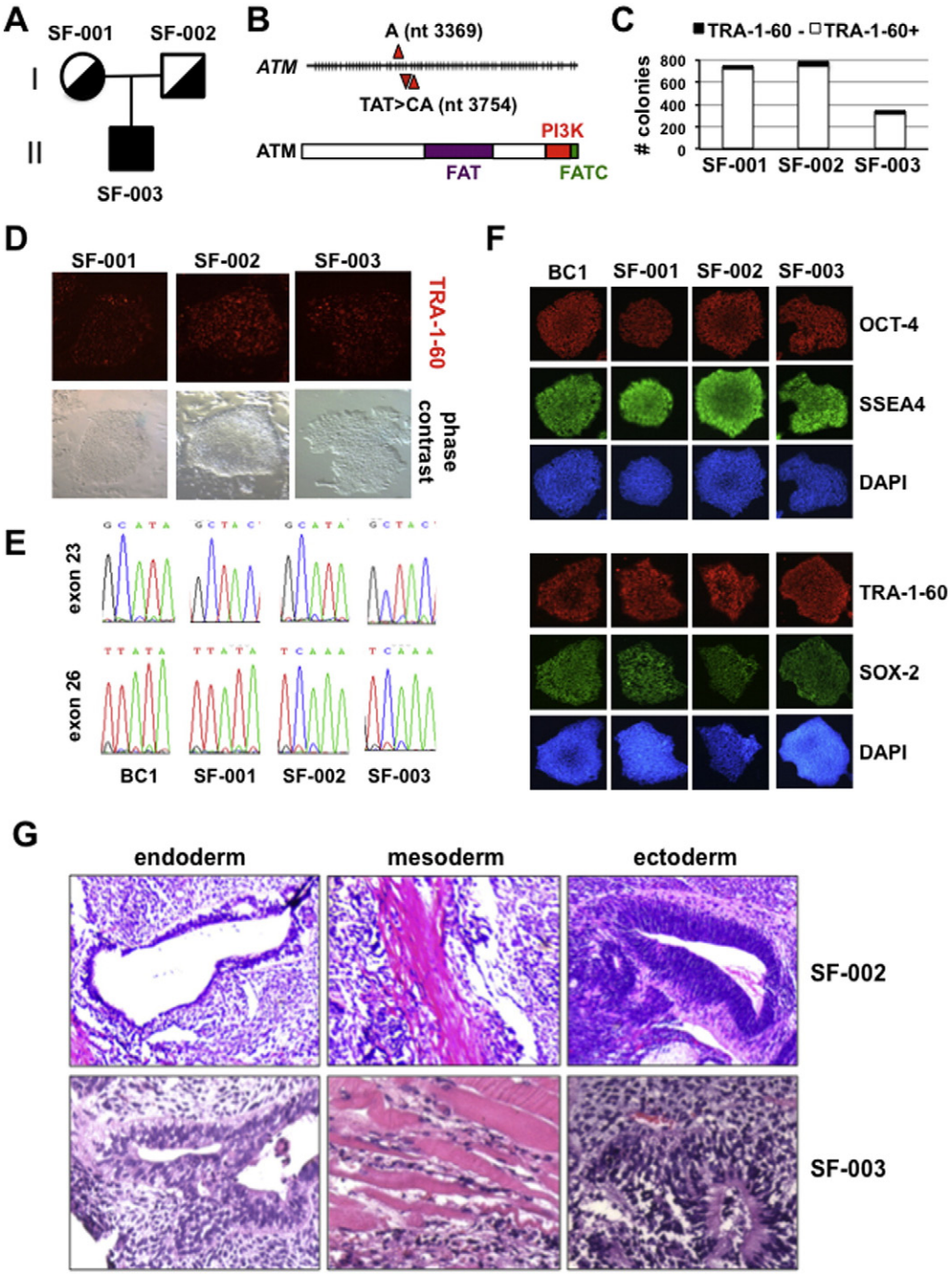

Fig. 1. Efficient generation of iPS cells from A-T and carrier erythroid cells. (A) Pedigree of the A-T family enrolled in this study. Blood was drawn from a male A-T patient and his carrier parents. The iPS cell lines derived from each individual are indicated. (B) Schematic of the ATM locus in human chromosome 11q22 and location of the mutations. A single nucleotide deletion in exon 23 and an indel in exon 26 are indicated. For both alleles, the mutated regions encode a poorly characterized region of the protein upstream of the catalytic domain (PI3K, depicted below). (C-D) To generate iPS cells, peripheral blood was briefly expanded *in vitro* and transfected with episomal vectors expressing Yamanaka factors. After 14 days, the total number of colonies and the number of TRA-1-60^{+} colonies were quantified. Representative examples of TRA-1-60^{+} colonies in each culture are shown in D. (E) Mutations were confirmed in genomic DNA of iPS cell lines by PCR amplification of target exons followed by cloning and sequencing of PCR products. Chromatograms of the mutation-containing regions are shown. BC1 is a control ATM$^{+/+}$ iPS cell line obtained from the bone marrow of a healthy individual. (F-G) To assess pluripotency, the indicated iPS cell lines were stained with antibodies to pluripotency markers OCT-4, SEEA4, TRA-1-60 and SOX-2 and counterstained with DAPI. Representative images of each line are shown in F. In addition, SF-002 and SF-003 iPS cell lines formed teratomas upon injection into the subcutaneous space of NGS mice. Representative images of H/E-stained teratomas sections are shown in G. See also Fig. S1.

reprogrammed the blood of the patient's parents, obligate A-T carriers. At day 14 after one-round transfection, we observed abundant iPS cell colonies in all three cultures (Fig. 1C for quantification, Fig. 1D for representative examples). Importantly, we observed a large number of colonies ($n = 343$) in the patient-derived culture and most (323/341; 94.7%) were positive for the pluripotency marker TRA-1-60 (Fig. 1C). Sequencing of gDNA from early-passage patient-derived SF-003iPS cells confirmed the expected compound heterozygous mutations (Fig. 1E). In addition, sequencing of early-passage SF-001 and SF-002 iPS cells established that the mutation in exon 23 was of maternal origin, while the mutation in exon 26 was paternal (Fig. 1E). Lines were further authenticated via STR profiling (Table S1). All lines were pluripotent, as single cells expressed pluripotency markers OCT4, SOX2, SSEA4 (Fig. 1E) and formed teratomas *in vivo* (Fig. 1G). Finally, analyses of gDNA from all iPS cell lines after amplification demonstrated that none of the three episomal vectors employed for expression of reprogramming factors had integrated in the iPS cell genome (Fig. S1). We conclude that reprogramming from A-T and carrier circulating erythroid cells expanded from a small volume of peripheral blood is not only feasible but highly efficient.

3.2. Erythroid-derived A-T iPS cells recapitulate features of A-T somatic cells

To further validate the patient-derived SF-003 iPS cell line, we first performed immunoblotting for ATM in extracts of early passage cells (Fig. 2A). A band of the expected size was detected in the control BC1 and parent-derived SF-001 and SF-002 iPS cell lines, but not in patient-derived SF-003 cells. Upon exposure to IR, ATM autophosphorylates to generate phospho-ATM (Ser1981) (Bakkenist and Kastan, 2003). Accordingly, we observed clear induction of phospho-ATM in extracts of BC1 or carrier cell lines, but none in extracts from patient-derived SF-003 cells (Fig. 2A). Altogether, these data indicate that the two frameshift mutations in SF-003 cells result in null alleles, validating this line as a model for the most common and severe form of A-T ("classical A-T").

In response to IR, ATM promotes activation of the DNA Damage Response (DDR) by phosphorylating a large number of substrates, including KAP-1 and p53 (Matsuoka et al., 2007). Consistent with previous findings in somatic cells (Goodarzi et al., 2008), phosphorylation of KAP1 (to form phospho-KAP1 Ser824) was markedly diminished in A-T SF-003 cells, while it appeared to be robust in haploinsufficient SF-001 and SF-002 cells (Fig. 2A). Similarly, we observed IR-induced p53 stabilization and phosphorylation at Ser15 (Canman et al., 1998) in BC1 and SF-002 cells, but not in patient-derived SF-003 cells (Fig. 2A). Unexpectedly, we found that carrier SF-001 iPS cells had no detectable p53 protein in baseline conditions and failed to form phospho-p53 (Ser15) or stabilize p53 after IR (Fig. 2A). In human tumors, p53 is often inactivated by missense mutations in exons 5 to 8, encoding the DNA binding domain. (Levine et al., 1991). However, our analyses of these exons in SF-001 gDNA revealed no mutations (Fig. S2), suggesting an alternative mechanism.

We next assessed the DDR in A-T iPS cells via analyses of IR-induced foci (IRIF) composition (Fig. 2B for quantification; Fig. 2C for representative examples). Consistent with the immunoblotting data above, SF-003

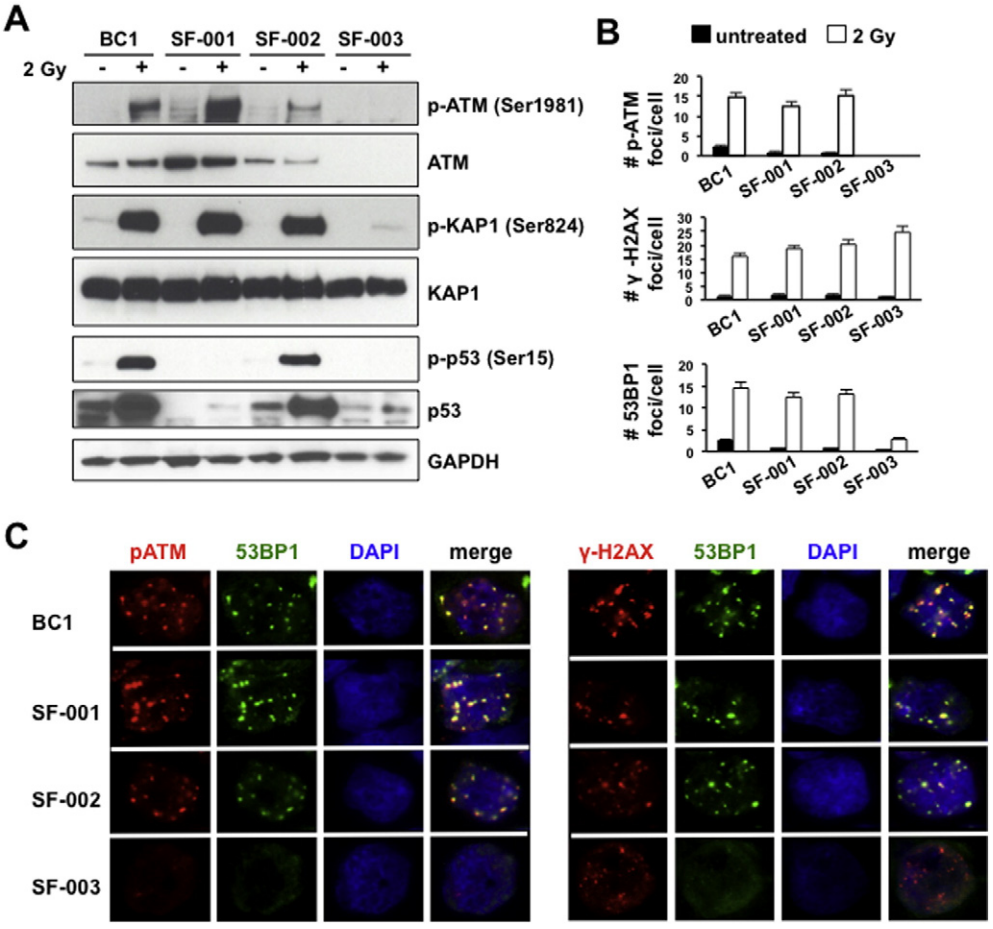

Fig. 2. Erytroid cell-derived A-T iPS cells recapitulate features of A-T somatic cells. (A) The indicated iPS cell lines were exposed to 2 Gy of IR or mock-irradiated. After one hour, protein extracts were immunoblotted with the indicated antibodies. (B-C) iPS cells were treated with 2 Gy of IR or mock-irradiated and fixed in 4% paraformaldehyde one hour after irradiation. Permeabilized cells were stained with antibodies to phospho-ATM (Ser1981), γ-H2AX or 53BP1 and counterstained with DAPI. Bars in (B) represent the average and s.e.m. for at least 50 cells per sample. Representative examples are shown in (C). See also Fig. S2.

cells failed to form phospho-ATM (Ser1981) IRIF, while SF-001 and SF-002 cells showed similar numbers as BC1 cells (14.7 ± 1.3, 12.3 ± 1.1 and 15.3 ± 1.5 foci per cell, respectively; Fig. 2B). In contrast, the number of γ-H2AX foci was comparable in ATM-deficient and proficient cells (15.7 ± 1.3, 18.7 ± 1.2, 20.2 ± 1.7 and 24.4 ± 2.1 γ-H2AX foci per cell for BC1, SF-001, SF-002 and SF-003 cells, respectively). This finding is consistent with previous observations in an independently generated A-T iPS cell line (Nayler et al., 2012) and previous findings in somatic cells (Stiff et al., 2004). In this context, DNA-PKcs and ATR are PI3K-like kinases that compensate for ATM in the formation of γ-H2AX foci (Stiff et al., 2004). However, IRIF formation was impaired in A-T iPS cells because IRIF containing 53BP1, an ATM substrate that regulates DSB repair pathway choice (Bunting et al., 2010), were markedly decreased after IR in SF-003 relative to control iPS cell lines (14.7 ± 1.3, 12.3 ± 1.1, 13.1 ± 1.2 and 2.8 ± 0.2 53BP1 foci per cell for BC1, SF-001, SF-002 and SF-003 cells, respectively; Fig. 2B-C). Altogether, these experiments indicate that A-T iPS cells recapitulate biochemical and cellular abnormalities in the activation of the DDR observed in A-T somatic cells, while A-T carrier iPS cells retain robust DDR activation.

3.3. Analysis of telomere length and capping function in erythroblast-derived A-T and carrier iPS cells

Telomere shortening with age is accelerated in primary A-T cells (Metcalfe et al., 1996). Consistent with these previous observations, flowFISH of lymphocytes and, to a lesser extent, granulocytes from the blood of the proband showed marked telomere attrition (Fig. S3). In contrast, telomere length of parental lymphocytes and granulocytes were within the normal range for their age (Fig. S3).

Telomere length is typically reset upon reprogramming (Suhr et al., 2009) due to re-expression of telomerase (Takahashi et al., 2007). To determine whether ATM may be limiting for telomere re-elongation in this context, we quantified telomere length in A-T and control cells by flowFISH (Fig. 3A). As expected, telomere length of the established BC1 iPS cell line remained stable over time (approximate telomere length, 8 kbp; Fig. 3A). In contrast, quantification of telomere length in patient-derived SF-003 cells revealed rapid telomere re-elongation after reprogramming (from 9.6 ± 0.2 kbp at P5 to 16.8 ± 0.3 kbp at P17; net gain, 7.2 kbp in 12 passages, or approximately 600 bp per passage; Fig. 3A). Similarly, average telomere length in the paternal carrier SF-002 line increased from 10.7 ± 0.3 at P5 to 16.9 ± 0.4 kbp at P17 (net gain, 6.2 kbp in 12 passages, or approximately 500 bp per passage; Fig. 3A). In contrast, parallel analysis of the carrier SF-001 iPS cells, deficient for p53 (Fig. 2A), revealed telomere shortening over time (net loss, 3.8 kbp in 12 passages; Fig. 3A). Because telomere maintenance is required for long-term self-renewal (Huang et al., 2011; Takahashi et al., 2007), we considered that SF-001 cells failed to meet criteria for pluripotency at initial evaluation and this line was not characterized further (see Discussion below).

To further characterize telomere function in *bona fide* iPS cell lines SF-002 and SF-003, we also examined the integrity of single chromosome ends via telomere FISH on metaphase spreads (Fig. 3B). For all lines, telomere length followed a normal distribution (357.1 ± 45.2, 303.3 ± 39.7 and 342.7 ± 66.6 arbitrary unit of fluorescence (a.u.f.) for BC1, SF-002 and SF-003 cells, respectively; $n = 10$ metaphases per line; Fig. 3B for histograms; Fig. S4 for representative images). Importantly, we found essentially no chromosome ends lacking telomere signal ("signal-free ends") or chromosome end-to-end fusions, two cytogenetic markers of telomere dysfunction (Kojis et al., 1991; Kojis et al., 1989) (Fig. 3B, Fig. S2).

The elongated, homogenous telomeres observed in BC1, SF-002 and SF-003 cells are consistent with telomere maintenance via telomerase. In support of this notion, we also found that hTERT, the catalytic subunit of telomerase and limiting factor for enzymatic activity (Bodnar et al., 1998), is highly expressed in all iPS cell lines (Fig. 3C). As controls, hTERT was undetectable in human primary fibroblasts (MRC5 cells), but readily detectable in the telomerase-positive cancer cell line HEK293T (Fig. 3C).

3.4. Erythroblast-derived A-T and carrier iPS cells have stable karyotypes and differentiate along the neural lineage

Our initial characterization above established that SF-002 and SF-003 represent *bona fide* iPS cell lines with potential utility to model neuronal function in A-T carriers and patients, respectively. To further validate these lines for preclinical studies, we first analyzed their karyotypes by G banding. As shown in Fig. 4A, both lines were euploid and lacked rearrangements, similar to previously reported fibroblast- or T cell-derived A-T iPS cell lines (Fukawatase et al., 2014; Lee et al., 2013; Lin et al., 2015; Nayler et al., 2012). To determine whether ATM is required for long-term maintenance of pluripotency, we analyzed gene expression at passage 17, after approximately 6 months in

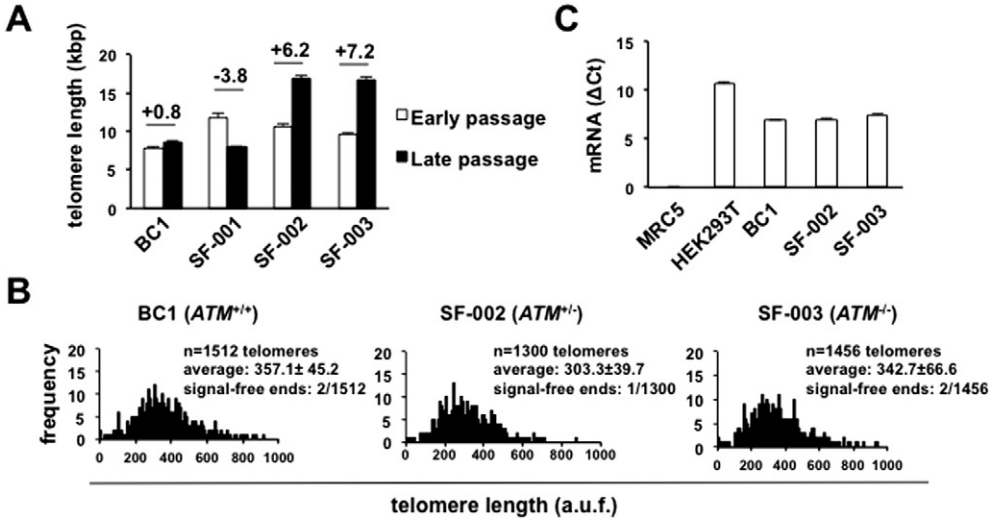

Fig. 3. Blood-derived A-T iPS cells reset telomere length. (A) Quantification of telomere length in the indicated iPS cell lines by flowFISH. SF-001, SF-002 and SF-003 lines were generated in parallel and assayed at P5 and P17. BC1 is a previously established line and was assayed at P45 and P58. Data are represented as mean and s.e.m. of three replicates. (B) Distribution of telomere length in the indicated lines by telomere FISH on metaphase spreads. SF-002 and SF-003 iPS cells were assayed at P8 and BC1 was assayed at P48. For all lines, 10 metaphases were analyzed. A.u.f., arbitrary units of fluorescence. (C) Quantitative RT-PCR for hTERT in iPS cell lines BC1, SF-002 and SF-003 and control MRC5 and HEK293T cells. mRNA expression represents the ΔCt relative to 18S RNA. Bars represent the average and standard deviation of 4 replicates. See also Figs. S3 and S4.

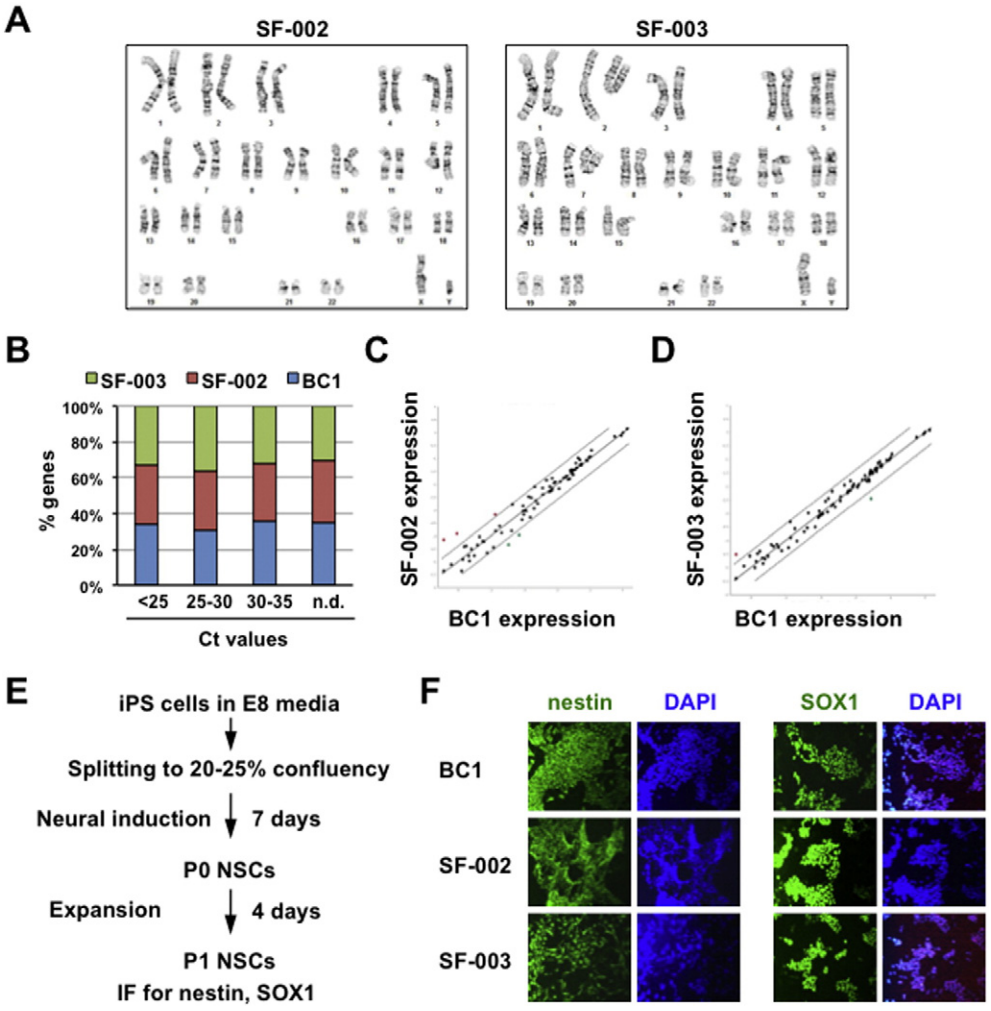

Fig. 4. A-T and carrier iPS cell lines maintain long-term pluripotency and differentiate along the neural lineage. (A) Metaphases spreads from SF-002 cells at P10 and SF-003 cells at P8 were karyotyped by G-banding. A representative example of 20 metaphases analyzed is shown. (B-D) Gene expression analyses of BC1, SF-002 and SF-003 cells using the RT^2 Profiler Array for Human Induced Pluripotent Stem Cells, enriched for pluripotency genes. Fig. 2B shows that the distribution of Ct values for all tested genes is similar for all iPS cell lines. The normalized expression of individual genes for lines SF-002 (C) and SF-003 (D) was plotted against the normalized expression of the same genes for the control BC1 line. (E-F) BC1, SF-002 and SF-003 cells were differentiated to NSCs using Neural Induction Media, briefly expanded, stained with antibodies to Nestin and SOX1 and counterstained with DAPI. The experimental protocol is summarized in (E) and representative images are shown in (F).

continuous culture, using a commercial PCR Array enriched for pluripotency genes (Fig. 4B-D). We found that pluripotency genes in the array were highly expressed in all lines, in contrast to the low levels of expression of genes that mark differentiation (Fig. 4B for distribution of expression levels (Ct values) per iPS cell line; Fig. 4C-D for expression of individual genes in SF-002 and SF-003 cells relative to expression of the same gene in BC1 cells, respectively).

Finally, we employed a commercially available modification of the dual SMAD inhibition protocol originally developed by the Studer Lab (Chambers et al., 2009) to assess the ability to differentiate to the neural lineage. In agreement with our finding of ectodermal tissue in iPS cell line-derived teratomas (Fig. 1G), all BC1, SF-002 and SF-003 cells readily differentiated to neural stem cells, as determined by expression of the intermediate filament protein nestin and the transcription factor SOX1, two widely employed neural stem cell (NSC) markers (Fig. 4E-F).

3.5. Effect of Atm haploinsufficiency on in vivo teratoma formation

In contrast to a previous report using fibroblasts (Nayler et al., 2012), haploinsufficiency for ATM does not appear to be a significant barrier to reprogramming in our conditions (see Fig. 1 above). However, our experimental system is not amenable to a standard colony-based quantitation assay. Moreover, individual genetic heterogeneity may mask an ATM gene dose effect. To examine the effect of ATM haploinsufficiency in a homogeneous genetic background, we took advantage of a recently developed C57BL/6 transgenic mouse that expresses Yamanaka factors ubiquitously upon addition of doxycycline to the drinking water (4iF mice) (Abad et al., 2013). Because most doxycycline-treated i4F mice succumb to teratomas during or within a short period of time after drug administration, survival can be used as an endpoint to assess the efficiency of reprogramming in different mutants.

We bred i4F mice to $Atm^{+/-}$ mice to generate a colony of 4iF/Atm$^{+/-}$ mice ($n = 12$) and control 4iF/Atm$^{+/+}$ littermates ($n = 8$) (see Fig. 5A for breeding scheme). $Atm^{-/-}$ control mice were not included in this study because they are highly prone to thymic lymphomas at a young age. At the end of a 10-week observation period, 6/8 4iF/Atm$^{+/+}$ and 7/12 4iF/Atm$^{+/-}$ mice had succumbed to teratomas (Fig. 5B for Kaplan Meier curve; Fig. 5C for examples of teratomas in necropsies of moribund animals). This survival difference was not statistically significant (log rank test, $p = 0.77$). In addition, necropsies of all surviving mice revealed teratomas in the abdomen of one 4iF/Atm$^{+/+}$ and one 4iF/Atm$^{+/-}$ mice. Overall, there was also no significant difference in the number, size or distribution of teratomas between the two groups.

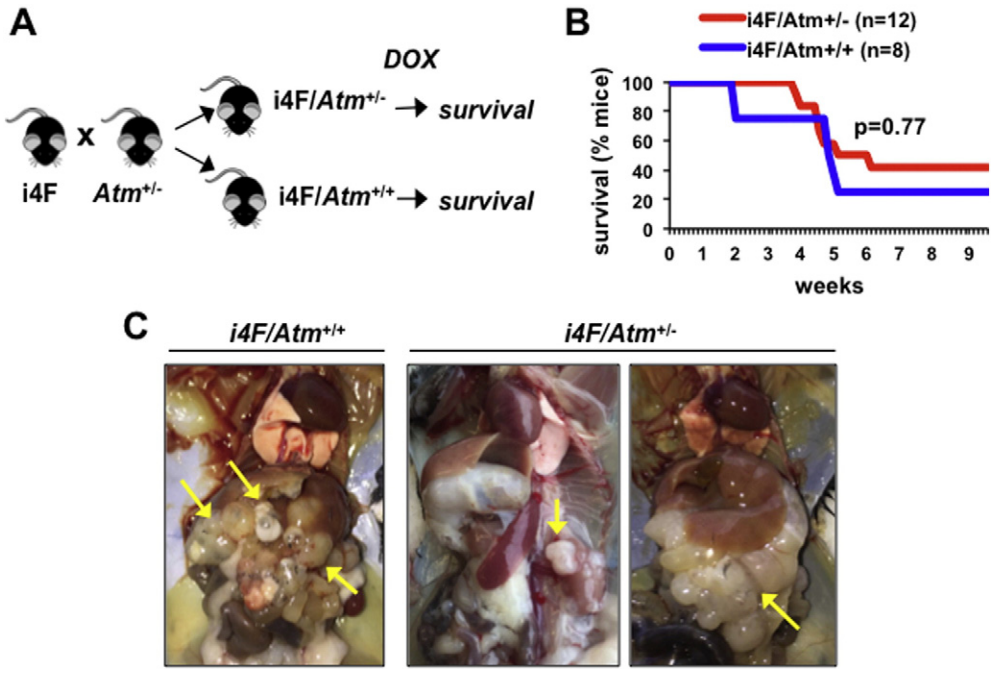

Fig. 5. Effect of ATM haploinsufficiency on teratoma formation *in vivo*. (A) Schematic of breedings for the generation of i4F mice with one or two copies of Atm. Upon exposure to doxycycline in the drinking water, survival was monitored as the endpoint for *in vivo* teratoma formation. (B) Kaplan Meier curve for cohorts of i4F/$Atm^{+/+}$ ($n = 8$) and i4F/$Atm^{+/-}$ ($n = 12$) mice. Doxycycline was administered in the drinking water during the first 2.5 weeks of the experiments. (C) Representative necropsies of moribund i4F/$Atm^{+/+}$ and i4F/$Atm^{+/-}$ mice. Yellow arrows point to teratomas.

4. Discussion

A-T, a monogenic disease presenting with multi-organ dysfunction early in childhood, is a candidate for regenerative medicine after gene defect correction. However, previous strategies to generate iPS cells from patient-derived somatic cells were hampered by very low reprogramming efficiency (fibroblasts) or possible contamination of the source with premalignant cells (T cells). Here, we show that circulating erythroid cells provide a robust and safe alternative for the generation of A-T iPS cells. Moreover, we find that reprogramming corrects defects in chromosomal integrity and telomere length observed in A-T somatic cells, suggesting that patient-derived iPS cells rather than somatic cells represent the best substrate for gene defect correction. This observation is not unique to A-T because a previous report demonstrated that the abnormal ring chromosome 17 causing Miller Dieker Syndrome (MDS) is also corrected by reprogramming (Bershteyn et al., 2014).

The use of patient peripheral blood for reprogramming has several advantages. First, the small volume of blood (30 cm^3 or less) employed here can be obtained from virtually any patient by venipuncture, obviating the need for specialized medical care and the discomfort associated to skin biopsies. Indeed, frozen material stored at a blood bank can be used. Secondly, the addition of BCl-xL to Yamanaka factors markedly increases the efficiency of reprogramming over previous findings using Yamanaka factors alone and fibroblasts (Fukawatase et al., 2014; Lee et al., 2013; Nayler et al., 2012). Importantly, the A-T line generated here has a normal karyotype, indicating that improved reprogramming efficiency does not result from unchecked proliferation of cells harboring chromosomal aberrations. Thirdly, our protocol takes advantage of the fact that, unlike the lymphoid compartment, the erythroid compartment is no or minimally affected in A-T, minimizing potential carry-over of abnormalities from parental cells. Finally, unlike most previous studies that employed feeder layers and/or viral vectors (Fukawatase et al., 2014; Lee et al., 2013; Lin et al., 2015; Nayler et al., 2012), our experiments were conducted using our previously described xeno-free episomal-based protocol (Chou et al., 2015), further supporting their clinical applicability.

Our work has also helped clarify the role for ATM in human cell telomere maintenance specifically in the context of reprogramming. The observations of accelerated telomere shortening (Metcalfe et al., 1996; Xia et al., 1996) and spontaneous telomere fusions in primary (Kojis et al., 1989, 1991) and transformed (Metcalfe et al., 1996; Pandita et al., 1995) somatic A-T cells led to the proposal that A-T is, at least in part, a syndrome of telomere dysfunction. Moreover, recent data indicates that ATM is required for telomerase-dependent telomere re-elongation is some contexts (Lee et al., 2015; Tong et al., 2015). In contrast, we find here that erythroblast-derived A-T iPS cells re-elongate telomeres to a length similar to that observed in human ES cells (Amit et al., 2000; Niida et al., 2000; Rosler et al., 2004), similar to a previous report on fibroblast-derived A-T iPS cells (Fukawatase et al., 2014). This observation has direct clinical relevance to regenerative medicine, as gene defect correction in the iPS cells would then restore telomere balance in their derived products. Consistent with previous findings in other iPS cell lines (Feng et al., 2010; Suhr et al., 2009; Vaziri et al., 2010), one carrier iPS cell line failed to maintain telomeres over time. These observations underscore the need to evaluate telomere dynamics in all newly generated iPS cell lines to assert pluripotency.

Finally, our work has also examined the effect of ATM gene dose by generating and analyzing an A-T carrier cell line from the patient's father. These experiments were motivated by the previous observation that, when using fibroblasts as a source, the efficiency of reprogramming in the mother of a patient was markedly decreased (Nayler et al., 2012). Furthermore, A-T carriers show decreased lifespan due to increased risk of cancer and cardiovascular disease (Su and Swift, 2000). Although our protocol does not allow for quantitative analysis of the reprogramming efficiency, we observed large numbers (over 700) of TRA-1-60^+ colonies in carrier cultures, suggesting no major defect in our experimental conditions. Furthermore, A-T carrier cells were comparable to a control iPS cell line generated from a healthy individual in all parameters assessed here, including activation of the DNA Damage Response, telomere maintenance and ability to maintain pluripotency and differentiate to the neural lineage. Finally, although murine cells deficient for ATM show severe reprogramming defects (Marion et al., 2009), we observed comparable *in vivo* teratoma formation in $Atm^{+/-}$

and control wild-type mice. Altogether, these findings indicate that, at least in some experimental conditions, heterozygocity for ATM does not represent a barrier to reprogramming.

5. Conclusions

Our results indicate that A-T erythroid cells represent a robust, safe source of iPS cells for disease modeling. Moreover, the findings here that A-T iPS cells have normal karyotype, re-elongate telomeres to embryonic-like length, maintain pluripotency with extended passage and differentiate along the neural lineage suggest that these cells may represent the optimal substrate for gene defect correction, towards the development of regenerative therapies for A-T. Finally, human and murine somatic cells from A-T carriers can be reprogrammed efficiently in the conditions tested here.

Author contributions

Niraj Bhatt: Collection and/or assembly of data, data analysis and interpretation, manuscript writing.

Rajib Ghosh: Collection and/or assembly of data, data analysis and interpretation, manuscript writing.

Sanchita Roy: Collection and/or assembly of data, data analysis and interpretation, manuscript writing.

Yongxing Gao: Collection and/or assembly of data, data analysis and interpretation, manuscript writing.

Mary Armanios: Conception and design, financial support, collection and/or assembly of data, data analysis and interpretation, manuscript writing.

Linzhao Cheng: Conception and design, financial support, data analysis and interpretation, manuscript writing.

Sonia Franco: Conception and design, financial support, collection and/or assembly of data, data analysis and interpretation, manuscript writing.

Funding sources

This work was supported by the Maryland Stem Cell Research Fund (grant number 2014-MSCRFE-0629) to S.F. and by Commonwealth Foundation funds to M.A.

Disclosure of potential conflict of interest

The authors do not have any potential conflict of interest.

Acknowledgements

We are most grateful to the A-T patient and his parents for their generous donation of blood for these studies and to Dr. Howard Lederman, Dr. Thomas Crawford, Jenny Wright and Renee Allard at the Johns Hopkins Children's Center A-T Clinic for assistance with patient selection, consent and blood collection. We also thank Terry Cadwell, Dr. Howard Lederman and Dr. Larry Kleinberg for invaluable assistance with IRB protocol preparation. We are grateful to Dr. Vidya Sagar Hanumanthu for help with the telomere length studies; Dr. Ie-Ming Shih for assistance with teratoma analysis and to Dr. Vasiliki Machairaki for critical reading of the manuscript.

Appendix A. Supplementary data

Supplementary data to this article can be found online at http://dx.doi.org/10.1016/j.scr.2016.08.006.

References

Abad, M., Mosteiro, L., Pantoja, C., Canamero, M., Rayon, T., Ors, I., Grana, O., Megias, D., Dominguez, O., Martinez, D., et al., 2013. Reprogramming in vivo produces teratomas and iPS cells with totipotency features. Nature 502, 340–345.

Alder, J.K., Stanley, S.E., Wagner, C.L., Hamilton, M., Hanumanthu, V.S., Armanios, M., 2015. Exome sequencing identifies mutant TINF2 in a family with pulmonary fibrosis. Chest 147, 1361–1368.

Ambrose, M., Gatti, R.A., 2013. Pathogenesis of ataxia-telangiectasia: the next generation of ATM functions. Blood 121, 4036–4045.

Amit, M., Carpenter, M.K., Inokuma, M.S., Chiu, C.P., Harris, C.P., Waknitz, M.A., Itskovitz-Eldor, J., Thomson, J.A., 2000. Clonally derived human embryonic stem cell lines maintain pluripotency and proliferative potential for prolonged periods of culture. Dev. Biol. 227, 271–278.

Baerlocher, G.M., Vulto, I., de Jong, G., Lansdorp, P.M., 2006. Flow cytometry and FISH to measure the average length of telomeres (flow FISH). Nat. Protoc. 1, 2365–2376.

Bakkenist, C.J., Kastan, M.B., 2003. DNA damage activates ATM through intermolecular autophosphorylation and dimer dissociation. Nature 421, 499–506.

Barlow, C., Hirotsune, S., Paylor, R., Liyanage, M., Eckhaus, M., Collins, F., Shiloh, Y., Crawley, J.N., Ried, T., Tagle, D., et al., 1996. Atm-deficient mice: a paradigm of ataxia telangiectasia. Cell 86, 159–171.

Barlow, C., Ribaut-Barassin, C., Zwingman, T.A., Pope, A.J., Brown, K.D., Owens, J.W., Larson, D., Harrington, E.A., Haeberle, A.M., Mariani, J., et al., 2000. ATM is a cytoplasmic protein in mouse brain required to prevent lysosomal accumulation. Proc. Natl. Acad. Sci. U. S. A. 97, 871–876.

Beraldi, R., Chan, C.H., Rogers, C.S., Kovacs, A.D., Meyerholz, D.K., Trantzas, C., Lambertz, A.M., Darbro, B.W., Weber, K.L., White, K.A., et al., 2015. A novel porcine model of ataxia telangiectasia reproduces neurological features and motor deficits of human disease. Hum. Mol. Genet.

Bershteyn, M., Hayashi, Y., Desachy, G., Hsiao, E.C., Sami, S., Tsang, K.M., Weiss, L.A., Kriegstein, A.R., Yamanaka, S., Wynshaw-Boris, A., 2014. Cell-autonomous correction of ring chromosomes in human induced pluripotent stem cells. Nature 507, 99–103.

Boder, E., Sedgwick, R.P., 1958. Ataxia-telangiectasia; a familial syndrome of progressive cerebellar ataxia, oculocutaneous telangiectasia and frequent pulmonary infection. Pediatrics 21, 526–554.

Bodnar, A.G., Ouellette, M., Frolkis, M., Holt, S.E., Chiu, C.P., Morin, G.B., Harley, C.B., Shay, J.W., Lichtsteiner, S., Wright, W.E., 1998. Extension of life-span by introduction of telomerase into normal human cells. Science 279, 349–352.

Bunting, S.F., Callen, E., Wong, N., Chen, H.T., Polato, F., Gunn, A., Bothmer, A., Feldhahn, N., Fernandez-Capetillo, O., Cao, L., et al., 2010. 53BP1 inhibits homologous recombination in Brca1-deficient cells by blocking resection of DNA breaks. Cell 141, 243–254.

Callen, E., Jankovic, M., Difilippantonio, S., Daniel, J.A., Chen, H.T., Celeste, A., Pellegrini, M., McBride, K., Wangsa, D., Bredemeyer, A.L., et al., 2007. ATM prevents the persistence and propagation of chromosome breaks in lymphocytes. Cell 130, 63–75.

Canman, C.E., Lim, D.S., Cimprich, K.A., Taya, Y., Tamai, K., Sakaguchi, K., Appella, E., Kastan, M.B., Siliciano, J.D., 1998. Activation of the ATM kinase by ionizing radiation and phosphorylation of p53. Science 281, 1677–1679.

Carlessi, L., Fusar Poli, E., De Filippis, L., Delia, D., 2013. ATM-deficient human neural stem cells as an in vitro model system to study neurodegeneration. DNA Repair 12, 605–611.

Chambers, S.M., Fasano, C.A., Papapetrou, E.P., Tomishima, M., Sadelain, M., Studer, L., 2009. Highly efficient neural conversion of human ES and iPS cells by dual inhibition of SMAD signaling. Nat. Biotechnol. 27, 275–280.

Chou, B.K., Mali, P., Huang, X., Ye, Z., Dowey, S.N., Resar, L.M., Zou, C., Zhang, Y.A., Tong, J., Cheng, L., 2011. Efficient human iPS cell derivation by a non-integrating plasmid from blood cells with unique epigenetic and gene expression signatures. Cell Res. 21, 518–529.

Chou, B.K., Gu, H., Gao, Y., Dowey, S.N., Wang, Y., Shi, J., Li, Y., Ye, Z., Cheng, T., Cheng, L., 2015. A facile method to establish human induced pluripotent stem cells from adult blood cells under feeder-free and xeno-free culture conditions: a clinically compliant approach. Stem Cells Transl. Med. 4, 320–332.

Dowey, S.N., Huang, X., Chou, B.K., Ye, Z., Cheng, L., 2012. Generation of integration-free human induced pluripotent stem cells from postnatal blood mononuclear cells by plasmid vector expression. Nat. Protoc. 7, 2013–2021.

Feng, Q., Lu, S.J., Klimanskaya, I., Gomes, I., Kim, D., Chung, Y., Honig, G.R., Kim, K.S., Lanza, R., 2010. Hemangioblastic derivatives from human induced pluripotent stem cells exhibit limited expansion and early senescence. Stem Cells 28, 704–712.

Franco, S., Gostissa, M., Zha, S., Lombard, D.B., Murphy, M.M., Zarrin, A.A., Yan, C., Tepsuporn, S., Morales, J.C., Adams, M.M., et al., 2006. H2AX prevents DNA breaks from progressing to chromosome breaks and translocations. Mol. Cell 21, 201–214.

Fukawatase, Y., Toyoda, M., Okamura, K., Nakamura, K., Nakabayashi, K., Takada, S., Yamazaki-Inoue, M., Masuda, A., Nasu, M., Hata, K., et al., 2014. Ataxia telangiectasia derived iPS cells show preserved x-ray sensitivity and decreased chromosomal instability. Sci. Rep. 4, 5421.

Gonzalez, F., Georgieva, D., Vanoli, F., Shi, Z.D., Stadtfeld, M., Ludwig, T., Jasin, M., Huangfu, D., 2013. Homologous recombination DNA repair genes play a critical role in reprogramming to a pluripotent state. Cell Rep. 3, 651–660.

Goodarzi, A.A., Noon, A.T., Deckbar, D., Ziv, Y., Shiloh, Y., Lobrich, M., Jeggo, P.A., 2008. ATM signaling facilitates repair of DNA double-strand breaks associated with heterochromatin. Mol. Cell 31, 167–177.

Hu, K., Yu, J., Suknuntha, K., Tian, S., Montgomery, K., Choi, K.D., Stewart, R., Thomson, J.A., Slukvin, I.I., 2011. Efficient generation of transgene-free induced pluripotent stem cells from normal and neoplastic bone marrow and cord blood mononuclear cells. Blood 117, e109–e119.

Huang, J., Wang, F., Okuka, M., Liu, N., Ji, G., Ye, X., Zuo, B., Li, M., Liang, P., Ge, W.W., et al., 2011. Association of telomere length with authentic pluripotency of ES/iPS cells. Cell Res. 21, 779–792.

Kojis, T.L., Schreck, R.R., Gatti, R.A., Sparkes, R.S., 1989. Tissue specificity of chromosomal rearrangements in ataxia-telangiectasia. Hum. Genet. 83, 347–352.
Kojis, T.L., Gatti, R.A., Sparkes, R.S., 1991. The cytogenetics of ataxia telangiectasia. Cancer Genet. Cytogenet. 56, 143–156.
Lavin, M.F., 2008. Ataxia-telangiectasia: from a rare disorder to a paradigm for cell signalling and cancer. Nat. Rev. Mol. Cell Biol. 9, 759–769.
Lavin, M.F., 2013. The appropriateness of the mouse model for ataxia-telangiectasia: neurological defects but no neurodegeneration. DNA Repair 12, 612–619.
Lee, P., Martin, N.T., Nakamura, K., Azghadi, S., Amiri, M., Ben-David, U., Perlman, S., Gatti, R.A., Hu, H., Lowry, W.E., 2013. SMRT compounds abrogate cellular phenotypes of ataxia telangiectasia in neural derivatives of patient-specific hiPSCs. Nat. Commun. 4, 1824.
Lee, S.S., Bohrson, C., Pike, A.M., Wheelan, S.J., Greider, C.W., 2015. ATM Kinase Is Required for Telomere Elongation in Mouse and Human Cells. Cell Rep. 13, 1623–1632.
Levine, A.J., Momand, J., Finlay, C.A., 1991. The p53 tumour suppressor gene. Nature 351, 453–456.
Lin, L., Swerdel, M.R., Lazaropoulos, M.P., Hoffman, G.S., Toro-Ramos, A.J., Wright, J., Lederman, H., Chen, J., Moore, J.C., Hart, R.P., 2015. Spontaneous ATM Gene Reversion in A-T iPSC to Produce an Isogenic Cell Line. Stem Cell Rep. 5, 1097–1108.
Mali, P., Cheng, L., 2012. Concise review: Human cell engineering: cellular reprogramming and genome editing. Stem Cells 30, 75–81.
Marion, R.M., Strati, K., Li, H., Murga, M., Blanco, R., Ortega, S., Fernandez-Capetillo, O., Serrano, M., Blasco, M.A., 2009. A p53-mediated DNA damage response limits reprogramming to ensure iPS cell genomic integrity. Nature 460, 1149–1153.
Matsuoka, S., Ballif, B.A., Smogorzewska, A., McDonald III, E.R., Hurov, K.E., Luo, J., Bakalarski, C.E., Zhao, Z., Solimini, N., Lerenthal, Y., et al., 2007. ATM and ATR substrate analysis reveals extensive protein networks responsive to DNA damage. Science 316, 1160–1166.
McKinnon, P.J., 2012. ATM and the molecular pathogenesis of ataxia telangiectasia. Annu. Rev. Pathol. 7, 303–321.
Metcalfe, J.A., Parkhill, J., Campbell, L., Stacey, M., Biggs, P., Byrd, P.J., Taylor, A.M., 1996. Accelerated telomere shortening in ataxia telangiectasia. Nat. Genet. 13, 350–353.
Muguruma, K., Nishiyama, A., Ono, Y., Miyawaki, H., Mizuhara, E., Hori, S., Kakizuka, A., Obata, K., Yanagawa, Y., Hirano, T., et al., 2010. Ontogeny-recapitulating generation and tissue integration of ES cell-derived Purkinje cells. Nat. Neurosci. 13, 1171–1180.
Muguruma, K., Nishiyama, A., Kawakami, H., Hashimoto, K., Sasai, Y., 2015. Self-organization of polarized cerebellar tissue in 3D culture of human pluripotent stem cells. Cell Rep. 10, 537–550.
Nayler, S., Gatei, M., Kozlov, S., Gatti, R., Mar, J.C., Wells, C.A., Lavin, M., Wolvetang, E., 2012. Induced pluripotent stem cells from ataxia-telangiectasia recapitulate the cellular phenotype. Stem Cells Transl. Med. 1, 523–535.
Niida, H., Shinkai, Y., Hande, M.P., Matsumoto, T., Takehara, S., Tachibana, M., Oshimura, M., Lansdorp, P.M., Furuichi, Y., 2000. Telomere maintenance in telomerase-deficient mouse embryonic stem cells: characterization of an amplified telomeric DNA. Mol. Cell. Biol. 20, 4115–4127.
Oka, A., Takashima, S., 1998. Expression of the ataxia-telangiectasia gene (ATM) product in human cerebellar neurons during development. Neurosci. Lett. 252, 195–198.
Orsburn, B., Escudero, B., Prakash, M., Gesheva, S., Liu, G., Huso, D.L., Franco, S., 2010. Differential requirement for H2AX and 53BP1 in organismal development and genome maintenance in the absence of poly(ADP)ribosyl polymerase 1. Mol. Cell. Biol. 30, 2341–2352.
Pandita, T.K., Pathak, S., Geard, C.R., 1995. Chromosome end associations, telomeres and telomerase activity in ataxia telangiectasia cells. Cytogenet. Cell Genet. 71, 86–93.
Park, I.H., Zhao, R., West, J.A., Yabuuchi, A., Huo, H., Ince, T.A., Lerou, P.H., Lensch, M.W., Daley, G.Q., 2008. Reprogramming of human somatic cells to pluripotency with defined factors. Nature 451, 141–146.
Paull, T.T., 2015. Mechanisms of ATM Activation. Annu. Rev. Biochem.
Rechsteiner, M., von Teichman, A., Ruschoff, J.H., Fankhauser, N., Pestalozzi, B., Schraml, P., Weber, A., Wild, P., Zimmermann, D., Moch, H., 2013. KRAS, BRAF, and TP53 deep sequencing for colorectal carcinoma patient diagnostics. J. Mol. Diagn. 15, 299–311.
Rosler, E.S., Fisk, G.J., Ares, X., Irving, J., Miura, T., Rao, M.S., Carpenter, M.K., 2004. Long-term culture of human embryonic stem cells in feeder-free conditions. Dev. Dyn. 229, 259–274.
Savitsky, K., Bar-Shira, A., Gilad, S., Rotman, G., Ziv, Y., Vanagaite, L., Tagle, D.A., Smith, S., Uziel, T., Sfez, S., et al., 1995. A single ataxia telangiectasia gene with a product similar to PI-3 kinase. Science 268, 1749–1753.
Shiloh, Y., 2003. ATM and related protein kinases: safeguarding genome integrity. Nat. Rev. Cancer 3, 155–168.
Shiloh, Y., Ziv, Y., 2013. The ATM protein kinase: regulating the cellular response to genotoxic stress, and more. Nat. Rev. Mol. Cell Biol. 14, 197–210.
Stiff, T., O'Driscoll, M., Rief, N., Iwabuchi, K., Lobrich, M., Jeggo, P.A., 2004. ATM and DNA-PK function redundantly to phosphorylate H2AX after exposure to ionizing radiation. Cancer Res. 64, 2390–2396.
Su, Y., Swift, M., 2000. Mortality rates among carriers of ataxia-telangiectasia mutant alleles. Ann. Intern. Med. 133, 770–778.
Suhr, S.T., Chang, E.A., Rodriguez, R.M., Wang, K., Ross, P.J., Beyhan, Z., Murthy, S., Cibelli, J.B., 2009. Telomere dynamics in human cells reprogrammed to pluripotency. PLoS One 4, e8124.
Swift, M., Chase, C., 1983. Cancer and cardiac deaths in obligatory ataxia-telangiectasia heterozygotes. Lancet 1, 1049–1050.
Swift, M., Morrell, D., Cromartie, E., Chamberlin, A.R., Skolnick, M.H., Bishop, D.T., 1986. The incidence and gene frequency of ataxia-telangiectasia in the United States. Am. J. Hum. Genet. 39, 573–583.
Takahashi, K., Tanabe, K., Ohnuki, M., Narita, M., Ichisaka, T., Tomoda, K., Yamanaka, S., 2007. Induction of pluripotent stem cells from adult human fibroblasts by defined factors. Cell 131, 861–872.
Tao, O., Shimazaki, T., Okada, Y., Naka, H., Kohda, K., Yuzaki, M., Mizusawa, H., Okano, H., 2010. Efficient generation of mature cerebellar Purkinje cells from mouse embryonic stem cells. J. Neurosci. Res. 88, 234–247.
Taylor, A.M., Metcalfe, J.A., Thick, J., Mak, Y.F., 1996. Leukemia and lymphoma in ataxia telangiectasia. Blood 87, 423–438.
Tilgner, K., Neganova, I., Moreno-Gimeno, I., Al-Aama, J.Y., Burks, D., Yung, S., Singhapol, C., Saretzki, G., Evans, J., Gorbunova, V., et al., 2013. A human iPSC model of Ligase IV deficiency reveals an important role for NHEJ-mediated-DSB repair in the survival and genomic stability of induced pluripotent stem cells and emerging haematopoietic progenitors. Cell Death Differ. 20, 1089–1100.
Tong, A.S., Stern, J.L., Sfeir, A., Kartawinata, M., de Lange, T., Zhu, X.D., Bryan, T.M., 2015. ATM and ATR Signaling Regulate the Recruitment of Human Telomerase to Telomeres. Cell Rep. 13, 1633–1646.
Valentin-Vega, Y.A., Maclean, K.H., Tait-Mulder, J., Milasta, S., Steeves, M., Dorsey, F.C., Cleveland, J.L., Green, D.R., Kastan, M.B., 2012. Mitochondrial dysfunction in ataxia-telangiectasia. Blood 119, 1490–1500.
Vaziri, H., Chapman, K.B., Guigova, A., Teichroeb, J., Lacher, M.D., Sternberg, H., Singec, I., Briggs, L., Wheeler, J., Sampathkumar, J., et al., 2010. Spontaneous reversal of the developmental aging of normal human cells following transcriptional reprogramming. Regen. Med. 5, 345–363.
Wang, S., Wang, B., Pan, N., Fu, L., Wang, C., Song, G., An, J., Liu, Z., Zhu, W., Guan, Y., et al., 2015. Differentiation of human induced pluripotent stem cells to mature functional Purkinje neurons. Sci. Rep. 5, 9232.
Xia, S.J., Shammas, M.A., Shmookler Reis, R.J., 1996. Reduced telomere length in ataxia-telangiectasia fibroblasts. Mutat. Res. 364, 1–11.
Zhang, J., Tripathi, D.N., Jing, J., Alexander, A., Kim, J., Powell, R.T., Dere, R., Tait-Mulder, J., Lee, J.H., Paull, T.T., et al., 2015. ATM functions at the peroxisome to induce pexophagy in response to ROS. Nat. Cell Biol. 17, 1259–1269.